ELSEVIER

A New Approach for Remote Sensing of Canopy Absorbed Photosynthetically Active Radiation. II: Proportion of Canopy Absorption

*Louis Moreau** *and Zhanqing Li*†

The amount of photosynthetically active radiation (PAR) absorbed by canopy ($APAR_{CAN}$) is essential to the productivity of vegetation. Monitoring $APAR_{CAN}$ from space has been achieved through the retrievals of two quantities, namely, the PAR incident at the surface ($PAR_{SFC}\downarrow$) and the fraction of PAR intercepted by the canopy, FPAR. We propose a new approach that splits $APAR_{CAN}$ into the PAR absorbed in the surface layer below the top of the canopy ($APAR_{SFC}$) and the ratio of $APAR_{CAN}$ / $APAR_{SFC}$, RPAR. The method is introduced in two parts. Part I develops a simple parameterization that retrieves $APAR_{SFC}$ more readily and accurately than $PAR_{SFC}\downarrow$. Part II, presented in this paper, deals with the retrieval of RPAR. It is shown that RPAR can be derived as accurately and readily as FPAR. Hence, it is envisaged that the new approach offers an easier and more accurate means of estimating $APAR_{CAN}$ than the traditional one. As an investigation tool, a one-dimensional multistream and multilayer model of canopy radiative transfer is first formulated. Extensive canopy modeling is conducted with input parameters of large ranges to represent a variety of canopies and ground conditions. For vegetated land, RPAR is found to correlate well with FPAR and thus RPAR can be estimated from FPAR. RPAR is also related with the surface vegetation indices (VIs) such as NDVI, SAVI, and DVI. The relationships between RPAR and VIs are driven by the changes in leaf area index. They are not sensitive to the solar zenith angle and the fractions of direct and diffuse radiation, but to the optical properties of the canopy. The models for inferring RPAR from various VIs are given, together with the correction models to account for the dependencies of RPAR on time and cloud cover.

*Intermap Information Technologies Ltd., Ottawa, Ontario
†Canada Centre for Remote Sensing, Ottawa, Ontario

Address correspondence to Zhanqing Li, Canada Centre for Remote Sensing, 588 Booth St., Ottawa, Ontario, Canada, K1A 0Y7.
Received 19 August 1994; revised 7 April 1995.

INTRODUCTION

Solar radiation in the wavelength interval from about 400 nm to 700 nm is often referred to as photosynthetically active radiation (PAR). The PAR absorbed by vegetation, $APAR_{CAN}$, is the source of energy for photosynthesis. This energy drives primary production, the carbon cycle, and also constitutes a substantial amount of solar energy that modifies water and heat exchange between the surface and the atmosphere. Therefore, information on the amount of $APAR_{CAN}$ is required for the modeling and understanding of global biospheric processes. It can, for instance, be used to estimate the net primary productivity of plants and the assimilation rate of CO_2 due to photosynthesis (Prince, 1991; Sellers, 1985; Budyko, 1980).

Although *in situ* measurements of $APAR_{CAN}$ are possible, only satellites provide the spatial and temporal coverage required for the global monitoring of $APAR_{CAN}$. It is thus important to design a simple and accurate method to retrieve this parameter with current and future space-borne sensors. So far, the common approach for remote sensing of APAR is to estimate the amount of PAR incident at the surface above the top of the canopy (TOC), $PAR_{SFC}\downarrow$, and the fraction of the PAR absorbed by the canopy, FPAR, so that

$$APAR_{CAN} = FPAR \cdot PAR_{SFC}\downarrow \quad (1)$$

However, retrieving the amount of solar radiation reaching the ground from space is no trivial task (Cess and Vulis, 1989). One must find a way to distinguish the flux backscattered by the atmosphere, clouds, and the surface. This entails some *a priori* knowledge about the surface albedo, the amounts of the atmospheric constituents, and the optical properties of clouds. To circumvent these difficulties, Li and Moreau (1996) proposed an algorithm that estimate the amount of PAR absorbed by the surface below the TOC, $APAR_{SFC}$, from

REMOTE SENS. ENVIRON. 55:192–204 (1996)

Published by Elsevier Science, Inc.

0034-4257 / 96 / $15.00
SSDI 0034-4257(95)00098-L

Table 1. Statistics of the Relationships between FPAR and NDVI from Different Investigations

Slope	*Ordinate Intercept*	R^2	*Source*
1.06	−0.07	0.99	Goward and Huemmrich (1992)
1.164	−0.143	0.92	Myneni and Williams (1994)
1.408	−0.396	0.92[a]	Pinter (1993)
1.21	−0.04	0.99	Goward et al. (1994)
1.2679	−0.30900	0.730	Hall et al. (1992)[b]
2.2132	−0.68107	0.665	Hall et al. (1992)[c]

[a] This number is computed from the data shown in Figure 2. The number presented in Pinter (1993) is a so-called "adjusted R^2" that is not directly comparable to the values given by the other investigations.
[b] Using a helicopter mounted Spectron Engineering 590 spectrometer.
[c] Using a helicopter mounted Barnes modular multiband radiometer (MMR).

the PAR reflected at the top of the atmosphere (TOA). In contrast to $PAR_{SFC}\downarrow$, determination of $APAR_{SFC}$ requires information on much fewer parameters including the solar zenith angle (SZA), ozone, and aerosol. Retrieval of cloud parameters is completely discharged from this algorithm. The method can be used for both clear and cloudy skies. $APAR_{CAN}$ is then given by

$$APAR_{CAN} = RPAR \cdot APAR_{SFC}, \tag{2}$$

where RPAR is the ratio of the PAR absorbed by canopy only over the PAR absorbed by both the canopy and the underlying ground. RPAR is not independent of FPAR. Combining Eqs. (1) and (2), we have

$$\frac{FPAR}{RPAR} = \frac{APAR_{SFC}}{PAR_{SFC}\downarrow} = 1 - a_{PAR}, \tag{3}$$

where a_{PAR} is the PAR albedo at the TOC. For a well-developed canopy, a_{PAR} is generally smaller than 5%, and therefore RPAR is very close to FPAR. The difference between FPAR and RPAR is larger for space and thin canopies over bright surfaces, such as deserts, and snow-covered lands. These situations are, however, of little interest for APAR studies. In any case, if a_{PAR} is known, RPAR can be derived from FPAR. Links between planetary and surface albedos in different spectral bands were addressed by many investigators (Chen and Ohring, 1984; Koepke, 1989; Asrar and Myneni, 1993; Li and Garand, 1994; et al.).

There have been plenty of studies (Choudhury, 1987; Myneni et al., 1992; Goward and Huemmrich. 1992; Pinter, 1993; among others) investigating the relationship between FPAR and vegetation indices (VIs) determined from visible and near-infrared (NIR) measurements. Good correlation was found using data from both experiments (Hall et al., 1992; Pinter, 1993; Goward et al., 1994) and modeling (Goward and Huemmrich, 1992; Myneni and Williams, 1994). Linear relationships between FPAR and the normalized difference vegetation index (NDVI) were derived. Table 1 lists the numbers of slope, intercept, and the percentage of explained variance obtained by different investigators. The exceptionally good result obtained by Goward and Huemmrich (1992) is presumably due to the use of fixed model input data. Significantly large scatter exists in the result of Myneni and Williams, who took, into account the variations of input parameters. The numbers of Goward et al. (1994) are subject to large statistical uncertainties, since they are based on merely five samples. Dye and Goward (1993) developed a global distribution of FPAR using the equation of Goward and Huemmrich (1992) with the NDVI computed from the AVHRR measurements made by NOAA-7 and corrected for atmospheric effects.

Although all these investigations end up with linear equations, nonlinearity is discernible in many studies (e.g., Myneni and Williams, 1994). In fact, the linear relationship is often an approximation of the nonlinear correspondence between FPAR and NDVI for a limited range of variables. The nonlinearity arises from the fact that NDVI saturates earlier than the canopy absorptance (Myneni et al., 1992). Moreover, NDVI is sensitive to the background spectral reflectance (e.g., Goward and Huemmrich, 1992). Difference in soil reflectance may partially explain the discrepancies among the equations listed in Table 1. The soil-adjusted VI (SAVI) proposed by Huete (1988) reduces the sensitivity, which was also used by Pinter (1993) as a predictor of FPAR. Of course, other forms of VIs can also be related to FPAR such as the difference VI (DVI).

As for FPAR, RPAR can also be estimated directly from VIs. By definition, RPAR should be modified mainly by the greenness of the canopy. To this end, we developed a canopy radiative transfer model to explore the potential of various types of VIs in inferring RPAR. It is envisaged that the relationship between RPAR and a VI is as good as that between FPAR and the VI. Since we intend to find a general algorithm that can be applied to any surface type at any time of the growing season, particular attention is paid to the diversity of the ground reflectance, optical properties of the leaves, solar zenith angle, etc. Nevertheless, the applicability of the algorithm is limited by the assumptions and simplifications

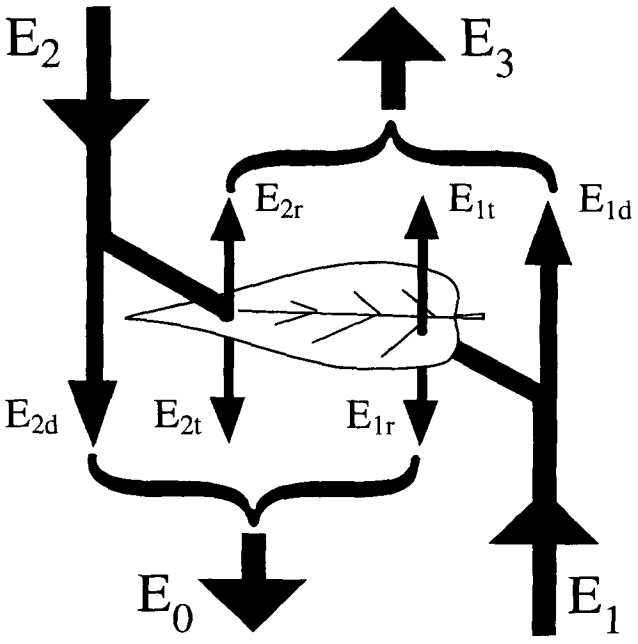

Figure 1. A schema of the canopy radiative transfer for various components of the solar fluxes.

made in the development of the radiative transfer model formulated in the next section.

CANOPY RADIATIVE TRANSFER MODEL

A one-dimensional (1D), multistream and multilayer model is developed that deals with the radiative transfer within a homogeneous canopy of uniform leaves with random leaf angle distribution (LAD). Use of such a simple model appears to suffice, according to the study of Myneni et al. (1992). By comparing the results of 1D with those of 3D models, they found that the relationship between NDVI and FPAR is not sensitive to the spatial distribution of leaves and heterogeneity; and that neglecting the hot spot effect and specular reflection from the leaves incurs errors smaller than 5% in the computation of FPAR, $APAR_{CAN}$, and NDVI. Moreover, our primary goal here is not to determine the characteristics of specific stands of vegetation but to correlate the absorption with the reflection of a canopy. Full 3D modeling that includes shadowing and other effects will not necessarily improve the results since the shaded parts of the canopy neither absorb nor reflect much radiation.

The model is designed based on the work of Norman (1979) and Verstraete (1987; 1988). The equations for a one-layer model are derived first and then generalized to constitute a multilayer model. Figure 1 is a schematic diagram showing the various components of the radiative energy transferring through a single-layer canopy. The total downward flux below the canopy, E_0, is the sum of the unintercepted downward flux E_{2d}, the transmitted downward flux E_{2t}, and the backscattered upward flux E_{1r}:

$$E_0 = E_{2d} + E_{2t} + E_{1r} \tag{4}$$

Similarly, the upward flux over the canopy is given by

$$E_3 = E_{1d} + E_{1t} + E_{2r}. \tag{5}$$

The fraction of the flux passing through the gaps in the canopy is (Norman, 1979)

$$E_{2d} = E_2 \cdot e^{-k_i\lambda} \tag{6}$$

and thus the intercepted flux is

$$E_2 - E_{2d} = E_2 (1 - e^{-k_i\lambda}), \tag{7}$$

where E_2 is the incoming flux at the TOC, k_i is the extinction coefficient associated with the incidence angle θ_i, and λ is the leaf area index (LAI) of the layer. The general expression for k_i is (Nilson, 1991)

$$k_i = G(\theta_i)\Omega / \cos\theta_i, \tag{8}$$

where Ω is the clumping factor and $G(\theta_i)$ is the mean projection of unit leaf area on the plane perpendicular to the beam direction θ_i from the normal to the ground. Ω and λ can be combined together to form an effective leaf area index (Black et al., 1991). For a uniform LAD (in both azimuth and zenith), $G(\theta_i)$ is equal to 0.5 (Norman, 1979). Taking those last two points into account, (8) becomes

$$k_i = 0.5 / \cos\theta_i. \tag{9}$$

The expression for E_{1d} is similar to (6)

The photons impinging on the foliage elements may be absorbed, transmitted, or reflected. The fractions of energy transmitted upward and downward, reflected upward and downward are obtained by multiplying the appropriate intercepted flux by the transmission and reflection coefficients, $\tau^{\uparrow}$, $\tau^{\downarrow}$, $\rho^{\uparrow}$, $\rho^{\downarrow}$ respectively. $\tau^{\uparrow}$, $\tau^{\downarrow}$, $\rho^{\uparrow}$, $\rho^{\downarrow}$, are functions of the reflectance and transmittance of the adaxial (subscript u) and abaxial (subscript d) side of the leaves, r_u, r_d, t_u, t_d, the LAD, and the incidence angle of the incoming flux. The general expressions for these coefficients for an incoming beam with angle θ_i are (Verstraete, 1988)

$$\rho^{\uparrow} = \int_0^{\pi/2} \left\{ \left[\left(\frac{\pi - \theta_L}{\pi} \right) r_u + \frac{\theta_L}{\pi} t_u \right] w_1 + \left[\left(\frac{\pi - \theta_L}{\pi} \right) t_d + \frac{\theta_L}{\pi} r_d \right] (1 - w_1) \right\} \sin\theta_L \, d\theta_L, \tag{10}$$

$$\tau^{\downarrow} = \int_0^{\pi/2} \left\{ \left[\left(\frac{\pi - \theta_L}{\pi} \right) t_u + \frac{\theta_L}{\pi} r_u \right] w_1 + \left[\left(\frac{\pi - \theta_L}{\pi} \right) r_d + \frac{\theta_L}{\pi} t_d \right] (1 - w_1) \right\} \sin\theta_L \, d\theta_L, \tag{11}$$

where θ_L is the leaf zenith angle. The equations for $\rho^{\downarrow}$ and $\tau^{\uparrow}$ are similar to (10) and (11) but with the subscripts

u and d interchanged. w_1 is the fractional number of leaves illuminated on their upper surfaces (Verstraete, 1987):

$$w_1 = \int_{-\varphi}^{+\varphi} f(\theta_L, \varphi_L)\, d\varphi_L \tag{12}$$

where $f(\theta_L, \varphi_L)$ is the LAD, φ_L is the leaf azimuth, and

$$\varphi = \arccos(-\cot\theta_i \cot\theta_L). \tag{13}$$

For a spherical distribution of LAD, uniform in both azimuth and zenith, $f(\theta_L, \varphi_L)$ is a constant, and $w_1 = \varphi/\pi$ or 0 if φ does not exist. It is a reasonable assumption that leaves are distributed uniformly in azimuth, whereas assuming a uniform LAD in zenith is simplistic and can be a poor approximation for some specific types of canopies. However, when a pixel covers a large area of mixed vegetation with unknown LAD, the spherical distribution is probably the best guess. At any rate, the relationship between the reflected and absorbed energy is not very sensitive to LAD (Myneni et al., 1992).

Applying Eqs. (6), (7), (9), and (10) to Eqs. (4) and (5) gives

$$E_0 = E_2\left[e^{-\lambda k_i} + \tau^{\downarrow}(1 - e^{-\lambda k_i})\right] + \rho^{\downarrow}E_1(1 - e^{-\lambda k_i}), \tag{14}$$

$$E_3 = E_1\left[e^{-\lambda k_i} + \tau^{\uparrow}(1 - e^{-\lambda k_i})\right] + \rho^{\uparrow}E_2(1 - e^{-\lambda k_i}). \tag{15}$$

The incoming flux at the TOC generally consists of direct and diffuse components. The fractions of the direct and diffuse fluxes are denoted by F and D, respectively, such that $F + D = 1$. Diffuse flux is divided into N_b streams over the zenith angle interval from 0° to 90°. The diffuse component may become anisotropic within and below the canopy after interacting with the vegetation, even if it is assumed to be isotropic at the TOC. Therefore, the diffuse flux is divided into several rays rather than using an average flux with an incidence angle of 60°. N_b is set to 6 in this study. The normalized total incoming flux can be written as:

$$E_2 = F + D = F + \sum_{i=1}^{N_b} 2D\,\Delta\theta \cos\theta_i \sin\theta_i, \tag{16}$$

where $\Delta\theta$ denotes the interval of zenith angle ($0.5\pi / N_b$).

Likewise, for E_0, E_1, and E_3, we have

$$E_0 = \sum_{i=0}^{N_b} E_{0i} = \sum_{i=0}^{N_b} E_{2di} + \sum_{i=1}^{N_b} E_{1ri} + \sum_{i=0}^{N_b} E_{2ti}, \tag{17}$$

$$E_1 = \sum_{i=1}^{N_b} E_{1i}, \tag{18}$$

$$E_3 = \sum_{i=0}^{N_b} E_{3i} = \sum_{i=0}^{N_b} E_{1di} + \sum_{i=0}^{N_b} E_{2ri} + \sum_{i=1}^{N_b} E_{1ti}. \tag{19}$$

The fraction of the surface reflected flux passing through the gaps between the foliage elements is given by

$$E_{1di} = E_{1i}e^{-\lambda k_i}. \tag{20}$$

If we neglect the specular reflection of the leaves, and assume that they act as isotropic diffusers, an equal amount of radiation is distributed in every reflected and transmitted ray:

$$E_{1ri} = 2\,\Delta\theta \cos\theta_i \sin\theta_i \sum_{i'=1}^{N_b} E_{1i'}(1 - e^{-\lambda k_{i'}})\rho_{i'}^{\downarrow}, \tag{21}$$

$$E_{1ti} = 2\,\Delta\theta \cos\theta_i \sin\theta_i \sum_{i'=1}^{N_b} E_{1i'}(1 - e^{-\lambda k_{i'}})\tau_{i'}^{\uparrow}. \tag{22}$$

The expressions for E_{2di}, E_{2ri}, and E_{2ti} are similar to (20), (21), and (22), respectively, so that (17) and (19) become

$$E_0 = \sum_{i=0}^{N_b} E_{0i} = Fe^{-k_i\lambda} + \sum_{i=1}^{N_b}\Bigg\{E_{2i}e^{-k_i\lambda} + 2\,\Delta\theta\cos\theta_i\sin\theta_i\Bigg[\sum_{i'=0}^{N_b}\tau_{i'}^{\downarrow}(1 - e^{-k_{i'}\lambda})E_{2i'} + \sum_{i'=1}^{N_b}\rho_{i'}^{\downarrow}(1 - e^{-k_{i'}\lambda})E_{1i'}\Bigg]\Bigg\}, \tag{23}$$

$$E_3 = \sum_{i=0}^{N_b} E_{3i} = \sum_{i=1}^{N_b}\Bigg\{E_{1i}e^{-k_i\lambda} + 2\,\Delta\theta\cos\theta_i\sin\theta_i \times\Bigg[\sum_{i'=1}^{N_b}\tau_{i'}^{\uparrow}(1 - e^{-k_{i'}\lambda})E_{1i'} + \sum_{i'=0}^{N_b}\rho_{i'}^{\uparrow}(1 - e^{-k_{i'}\lambda})E_{2i'}\Bigg]\Bigg\}. \tag{24}$$

If the ground is a Lambertian reflector with albedo, r_g, the boundary equations are given by

$$E_2 = F + D = F + \sum_{i=1}^{N_b} 2D\,\Delta\theta\cos\theta_i\sin\theta_i \equiv 1, \tag{25}$$

$$E_1 = \sum_{i=1}^{N_b} E_{1,i} = \sum_{i=1}^{N_b}(2\,\Delta\theta\, r_g \cos\theta_i \sin\theta_i E_0). \tag{26}$$

Eqs. (4)–(26) comprise a single-layer canopy model of radiative transfer. It can be generalized for a multilayer canopy to take into account multiscattering between the layers. The multilayer model is obtained by using the upward and downward fluxes from the underlying and overlying layers as input for the intermediate layer. The LAI for a single layer, λ_i, has to be small enough so the multireflection within the layer can be neglected. $\lambda_i = 0.1$ seems to be sufficient since using a smaller value does not produce any significant numerical difference.

The generalized equations for the downward and upward fluxes for a canopy of n layers are given by Eqs. (27)–(30), respectively. Note that subscript j refers to the layer number (0 being the ground and n being the TOC) and subscript i refers to the ray number (0 being the direct beam). The first subscript is even for downward fluxes and odd for upward fluxes. By this convention, we have

$$E_{2j-2,0} = E_{2j,0}e^{-k_0\lambda_j} \tag{27}$$

for the direct downward beam ($i = 0$),

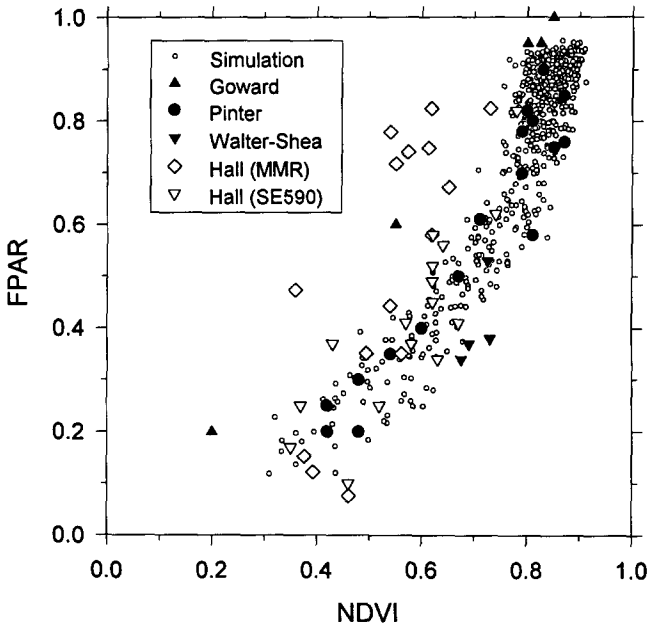

Figure 2. Comparison of the relationship between FPAR and NDVI obtained from canopy modeling with the observations reported in other studies.

$$E_{2j-2,i} = E_{2j,i}e^{-k_i\lambda_j} + 2\,\Delta\theta\cos\theta_i\sin\theta_i \times\left[\sum_{i'=0}^{Nb}\tau_{i'}^{\downarrow}(1-e^{-k_{i'}\lambda_j})E_{2j,i'} + \sum_{i'=1}^{Nb}\rho_{i'}^{\downarrow}(1-e^{-k_{i'}\lambda_j})E_{2j-1,i'}\right] \quad (28)$$

for the diffuse downward rays ($1 \leqslant i \leqslant N_b$),

$$E_{2j+1,0} = 0 \quad (29)$$

for the direct upward beam ($i = 0$), and

$$E_{2j+1,i} = E_{2j-1,i}e^{-k_i\lambda_j} + 2\,\Delta\theta\cos\theta_i\sin\theta_i \times\left[\sum_{i'=1}^{Nb}\tau_{i'}^{\uparrow}(1-e^{-k_{i'}\lambda_j})E_{2j-1,i'} + \sum_{i'=0}^{Nb}\rho_{i'}^{\uparrow}(1-e^{-k_{i'}\lambda_j})E_{2j,i'}\right] \quad (30)$$

for the diffuse upward rays ($1 \leqslant i \leqslant N_b$).

The boundary conditions at the TOC are given by

$$E_{2n,0} = \mathrm{F}, \quad (31)$$

$$E_{2n,i} = 2D\,\Delta\theta\cos\theta_i\sin\theta_i \quad \text{for } 1 \leqslant i \leqslant N_b \quad (32)$$

and at the bottom

$$E_{1,0} = 0, \quad (33)$$

$$E_{1,i} = 2\Delta\theta\, r_g\cos\theta_i\sin\theta_i\sum_{i'=0}^{Nb}E_{0,i'} \quad \text{for } 1 \leqslant i \leqslant N_b. \quad (34)$$

For n layers and N_b streams, the model is a set of $2(n+1)(N_b+1)$ linear equations that can be solved with a standard matrix method.

The reflectance and the absorptance of the canopy are

$$R_{\mathrm{TOC}} = \sum_{i=0}^{Nb}E_{2n+1,i}, \quad (35)$$

$$A_c = 1 - R_{\mathrm{TOC}} - A_g, \quad (36)$$

respectively, where A_g is the absorptance of the soil given by

$$A_g = \sum_{i=0}^{Nb}E_{0,i} - \sum_{i=0}^{Nb}E_{1,i}. \quad (37)$$

So, RPAR and FPAR are computed by

$$\mathrm{RPAR} = \frac{A_c}{A_c + A_g}, \quad (38)$$

$$\mathrm{FPAR} = A_c, \quad (39)$$

where A_c and A_g are given in the PAR spectral band. VIs are calculated using R_{TOC} in the visible and NIR bands. Three types of VI are investigated including NDVI, SAVI, and DVI, which are defined by

$$\mathrm{NDVI} = \frac{R_{\mathrm{TOC2}} - R_{\mathrm{TOC1}}}{R_{\mathrm{TOC2}} + R_{\mathrm{TOC1}}}, \quad (40)$$

$$\mathrm{DVI} = R_{\mathrm{TOC2}} - R_{\mathrm{TOC1}}, \quad (41)$$

$$\mathrm{SAVI} = \frac{R_{\mathrm{TOC2}} - R_{\mathrm{TOC1}}}{1.5\,(R_{\mathrm{TOC2}} + R_{\mathrm{TOC1}} + 0.5)}, \quad (42)$$

where the subscripts 1 and 2 refer to the visible and NIR bands, respectively.

As a reliability check of our canopy radiative transfer model, the modeling relationship between FPAR and NDVI is compared with the field measurements made

Table 2. Input Parameters and Their Range of Variation Used for the Radiative Transfer Modeling

Quantity	*Symbol*	*Range of Values*
Total effective leaf area index	Λ	0.1–6.0
Solar zenith angle	θ_s	0–85°
Ground reflectance in the visible	r_{g1}	0.05–0.20
Ground reflectance in the NIR	r_{g2}	r_{g1} + [0.1, 0.5] r_{g1}
Reflectance of the leaves, in the visible	r_1	0.05–0.10
Transmittance of the leaves in the visible	t_1	0.05–0.10
Reflectance of the leaves, in the NIR	r_2	0.35–0.55
Transmittance of the leaves in the NIR	t_2	0.45–0.55[a]

[a] t_2 is limited to a maximum value of $1 - r_2$.

by Goward et al. (1994) in Oregon for various canopy types, Pinter (1993) for alfalfa, Hall et al. (1992) at the FIFE sites with two different instruments, and Walter-Shea et al. (1992) for tallgrass fields. We use FPAR instead of RPAR simply because no RPAR observations were reported in the publications. Figure 2 shows that the relationship formed by the observations agrees well with the simulations. Except for one point from the data of Goward et al. (1994) and some of the data compiled by Hall et al. (1992) using the Barnes modular multiband radiometer (MMR), all of the observations fall well within the cluster of simulation points. Although the limited number of experimental samples may not be sufficient to fully validate the model, it lends us some confidence in it.

DETERMINATION OF RPAR

More than 500 simulations were made using the canopy radiative transfer model described above with random input parameters of the ranges delineated in Table 2 The ranges of the optical properties of leaves are based on Sellers (1985), Walter-Shea and Norman (1991), Goward et al. (1994, and Brakke et al. (1993), which cover many species during the growing season. The optical properties of the adaxial and abaxial sides of the leaves are considered identical. The fractions of incoming direct fluxes in the visible and NIR, F_1 and F_2, are determined by an atmospheric radiative transfer model (Masuda et al., 1995) for a cloudless sky with the CONT-I aerosol (WCP, 1986) for varying optical thickness ranging from 0 to 1. Both F_1 and F_2 depend strongly on the solar zenith angle and aerosol optical thickness (Fig. 3). Nevertheless, the specific choice of the values of F_1 and F_2 does not affect the relationship between RPAR and VI, as will be shown later.

It was stated earlier that the magnitudes of FPAR and RPAR are expected to be similar in the regions of interest for APAR studies (i.e., when and where the ground is covered by a moderate amount of vegetation). This is further confirmed by the results of canopy radiative transfer simulations shown in Figure 4. It appears that RPAR and FPAR are not only close to each other but also well correlated by the following equation:

$$\text{RPAR} = 1.05\,\text{FPAR} \quad (R^2 = 0.998, \quad \sigma = 0.01), \quad (43)$$

where σ is the standard deviation of the fitting errors. The small value of σ suggests that the accuracy of the estimate of RPAR based solely on FPAR is acceptable for most vegetated land, even when the surface PAR albedo is unknown. The significance of this finding rests on the fact that there have been extensive studies on the determination of FPAR as outlined in the introduction.

For the sake of estimating RPAR from VIs, the relationship between RPAR and different VIs (DVI, NDVI, and SAVI) at the TOC are established using the

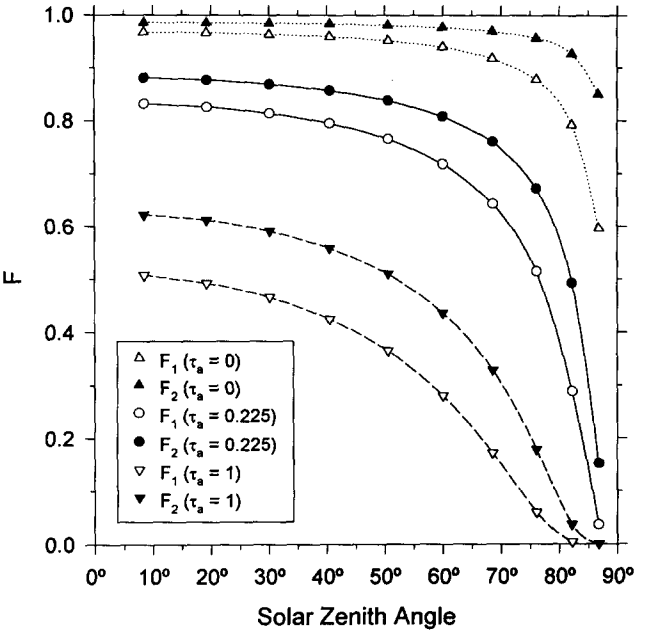

Figure 3. Fractions of the direct radiation out of the total radiation in the visible (F_1) and the NIR (F_2) wavelengths incident at the top of canopy as functions of the solar zenith angle for the standard midlatitude summer atmosphere with the CONT-I aerosol of varying optical thickness indicated by τ_a.

simulation results presented in Figure 5. Note that the variation of RPAR is roughly proportional to the changes in VIs. Each of the VIs has its strength and weakness for predicting RPAR. NDVI has a large range of variation, but it becomes saturated at around 0.8. As a result,

Figure 4. Comparison between RPAR and FPAR simulated by canopy modeling with random input parameters varying within the ranges delineated in Table 2.

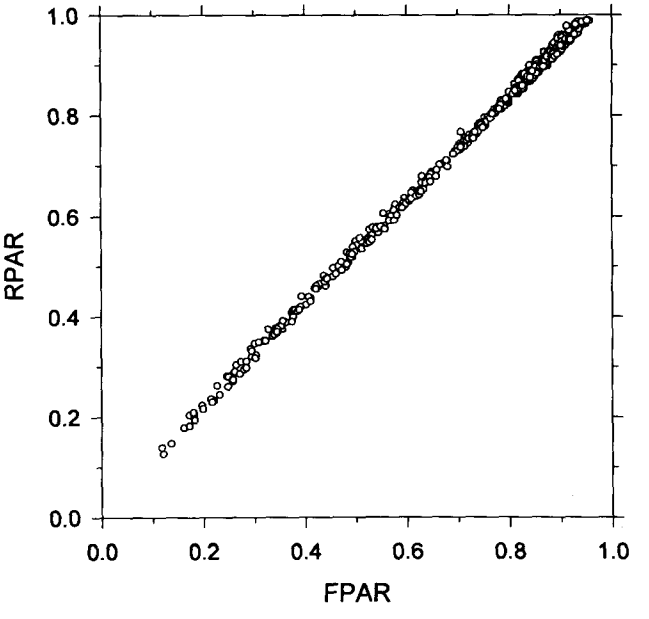

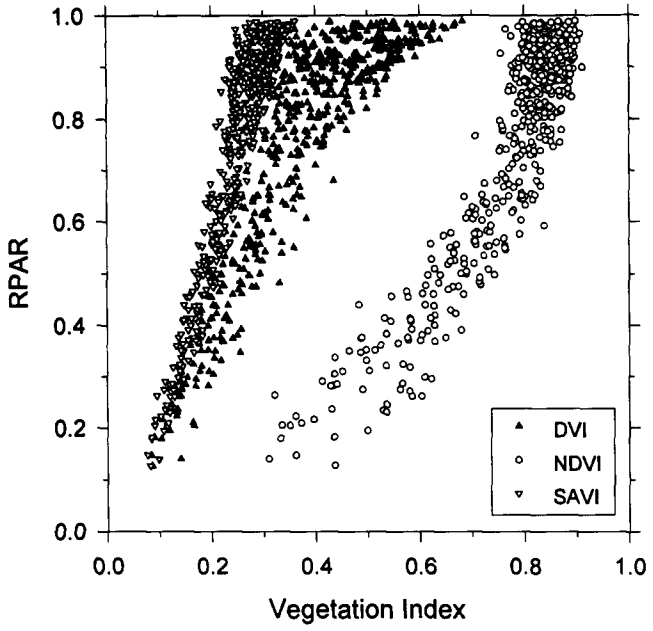

Figure 5.. The relationships between RPAR and various vegetation indices (NDVI, DVI, and SAVI) obtained from canopy modeling with random input data.

the relationship between RPAR and NDVI is not linear, unless smaller ranges are considered. In comparison, SAVI has a more or less constant slope with a magnitude, however, so high that a large range of RPAR corresponds to a fixed value of SAVI. The relationship between RPAR and DVI has a large slope and large spread and is thus excluded from further analysis. On the basis of these simulation results, regressional relationships between RPAR and NDVI, RPAR and SAVI are obtained:

$$\text{RPAR} = 0.105 - 0.323\ \text{NDVI} + 1.468\ \text{NDVI}^2 \quad (R^2 = 0.85,\ \sigma = 0.090), \tag{44}$$

$$\text{RPAR} = -0.070 + 3.257\ \text{SAVI} \quad (R^2 = 0.86,\ \sigma = 0.083). \tag{45}$$

Note that the above equations should be used with the constraint that RPAR ranges from 0 to unity. Besides, Eq. (44) is valid for NDVI $\geq$ 0.2.

The histogram of the differences between the values of RPAR computed with the canopy model and given by Eqs. (44) and (45) are displayed in Figures 6a and 6b for NDVI and SAVI, respectively. For 90% of the 516 simulated cases, the estimates of RPAR from SAVI and NDVI are accurate to within ± 0.12 and ± 0.14, respectively, of the corresponding simulated RPAR. It is worth noting that an accuracy of ± 0.1 in FPAR is considered acceptable for agronomical applications (Clevers et al., 1994). Considering that APAR_{SFC} can be determined more accurately than the downwelling PAR (Li and Moreau, 1995), the requirement for RPAR

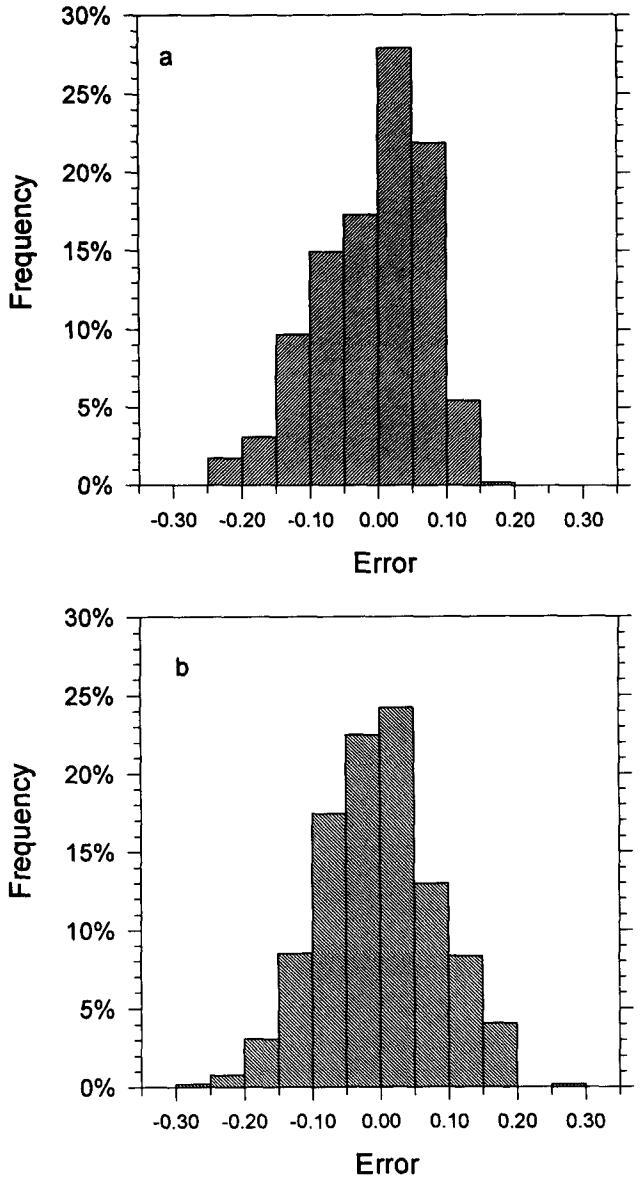

Figure 6.. Histograms of the differences in RPAR between the canopy modeling and estimation from SAVI (a) and NDVI (b) using the regression Eqs. (44) and (45).

should be less rigorous than FPAR to achieve the same accuracy in the estimate of the PAR absorbed by the canopy. Therefore, the relationships given by Eqs. (44) and (45) are adequate for deriving RPAR from SAVI and NDVI.

SENSITIVITY TESTS

The data points of Figure 5 are quite dispersed resulting from the use of wide ranges for input data. While this ensures the generality of the relationships between RPAR and VIs, the responses of the relationships to changes in input parameters are obscured. Sensitivity tests are therefore conducted to reveal the effects of

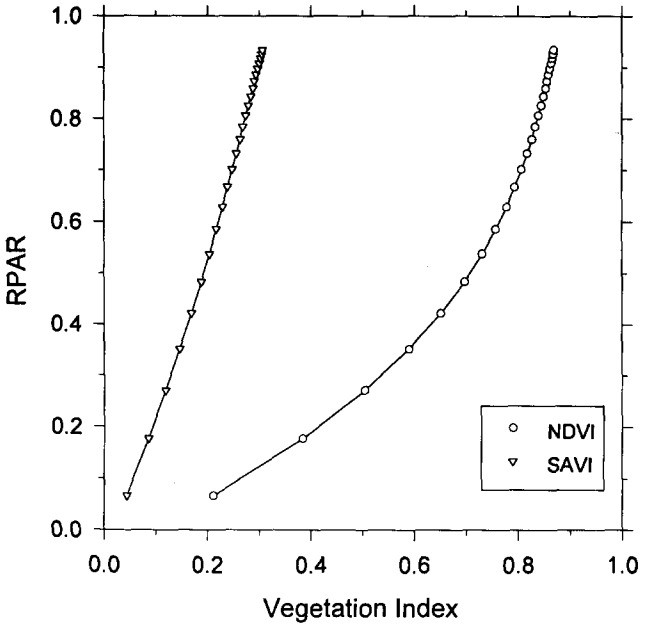

Figure 7. The relationships between RPAR and the vegetation indices of NDVI and SAVI obtained from canopy modeling for fixed input data except leaf area index. The input parameters are $r_{g1} = 0.10$, $r_{g2} = 0.12$, $r_1 = 0.084$, $r_2 = 0.442$, $t_1 = 0.059$, $t_2 = 0.514$, $\theta_s = 30°$, $\tau_a = 0.225$.

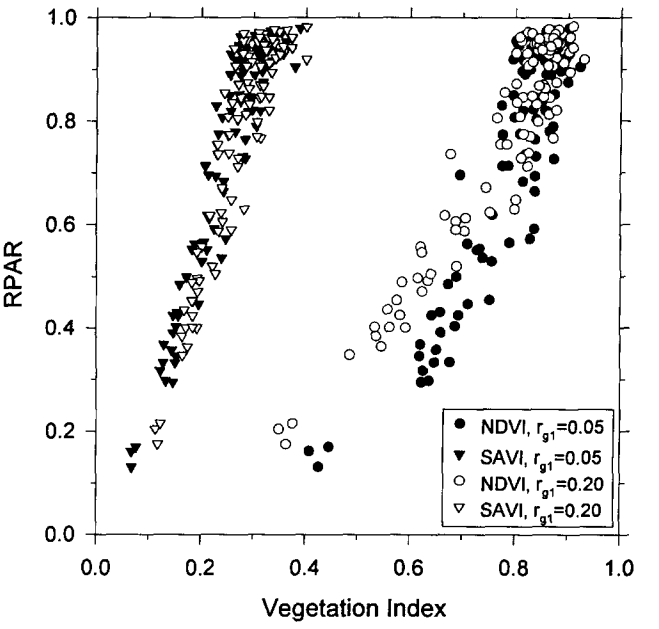

Figure 8. Same as Figure 7 except using random numbers for all the input parameters within the ranges given in Table 2 but for fixed ground reflectance at 0.05 (solid points) and 0.20 (open points) in the visible band and 0.06 and 0.30 in the NIR.

individual input parameters. The input parameters to be tested include LAI, surface reflectance, SZA, leaf optical properties, and aerosol optical thickness. Changes in the SZA and aerosol modify the components of direct and diffuse incoming radiation at the TOC.

The two smooth curves displayed in Figure 7 represent the variation of RPAR with SAVI and NDVI in response solely to the changes of LAI. Comparing Figure 7 with Figure 4 reveals that it is the LAI that drives the corresponding relationships between RPAR and the VIs and the variations of other parameters are a source of spread to the relationships. Figure 8 shows two series of simulations with the same random numbers for all input parameters but with ground reflectance set to 0.05 and 0.2. The difference in the relationship between RPAR and NDVI for the two sets of input data is considerable, especially when RPAR < 0.6. The values of NDVI for brighter soil are systematically smaller than those for darker soil. Consequently, large uncertainties may occur in the estimates of RPAR from NDVI over open canopies with various soil types of unknown albedos. The effect of soil reflectance is imperceptible on the relationship between RPAR and SAVI. This is expected because SAVI is designed to suppress the sensitivity to ground albedo. Figures 9 and 10 are similar to 8 but for the SZA and aerosol optical thickness. Although the data points in Figures 9 and 10 are displaced when the values of the SZA and the aerosol optical thickness are modified, the distributions of the data points harmonize well, suggesting that the relationships between RPAR and VIs are not affected by these two variables. As both the SZA and aerosol optical thickness modulate strongly the ratio of direct to total radiation, the relationship must be independent of the ratio. The independency of the SZA in the relationship between FPAR and the measured TOC VIs was also noted by Pinter (1993). In Figure 11, all input parameters are fixed but the optical properties of the leaves are allowed to vary randomly within the ranges given in Table 2. The degree of the spread is comparable to that appearing in Figure 4, implying that the changes in the spectral reflectance and transmittance of the leaves contribute substantially to the scatter of Figure 4. Goward et al. (1994) also noted the importance of the optical properties of the leaves in altering the relationship between FPAR and NDVI. In summary, it is the variations in soil reflectance and leaf optical properties that cause the dispersion in the relationships between RPAR and the VIs. It is thus imperative that any relationship for general application be derived for various surfaces and vegetation types. For the same reason, it is expected that an empirical relationship derived from field measurements made over a specific site may not hold for other sites or even for the same site at different times in the growing season.

ADJUSTING RPAR FOR CLOUD COVER DEPENDENCY

While the relationships between RPAR and VIs do not depend on the ratio of direct to total incoming radiation,

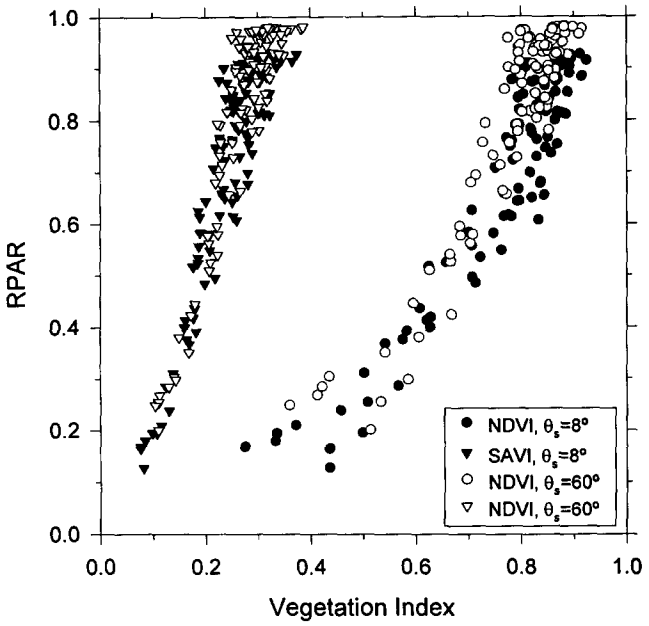

Figure 9. Same as Figure 8 but for the fixed solar zenith angles of 8° (solid points) and 60° (open points).

F, both RPAR and VI are functions of F. Figure 12 shows the variation of RPAR with F in the visible band, F_1, for a fixed set of canopy parameters. It follows that the dependency of RPAR on F_1 is linear and the slope is altered by the SZA. When SZA is large, RPAR increases with F_1. For a SZA = 80°, RPAR increases considerably from clear sky (large F_1) to overcast conditions ($F_1 = 0$). For small SZAs, RPAR diminishes with F_1. For intermediate values of SZA (around 60°), RPAR varies little with F_1. A similar linear relationship was found by Goward et al. (1994) for FPAR. The dependence on the SZA is lost under such overcast conditions that have no direct incoming flux.

In addition to the SZA, the slope is also modified by the optical properties of the canopy and underlying ground. Such an influence can be accounted for by the clear-sky RPAR, since its value for a given SZA is determined by these properties. Figure 13 is a 3D plot showing the variation of the slope with the cosine of the SZA and RPAR obtained from 400 clear-sky simulations with random input data. The following equation fits well the slope s delineated in Figure 13 with a multiple correlation coefficient 0.99 and a standard deviation of the fitting errors $\sigma = 0.023$:

$$s = 0.39 - 0.19\mu \ln(\mu) - 2.36\sqrt{\mathrm{RPAR}_{\mathrm{clear}}} + 1.27\sqrt{\mu\,\mathrm{RPAR}_{\mathrm{clear}}} + 1.70e^{-\mu/\mathrm{RPAR}_{\mathrm{clear}}}, \quad (46)$$

where μ is the cosine of the SZA.

Owing to the dependency on cloud cover through F_1, RPAR measured on a clear day has to be adjusted for use on cloudy days. Knowing the slope, RPAR for a cloudy sky, $\mathrm{RPAR}_{\mathrm{cloudy}}$, can be computed from a clear-sky RPAR, $\mathrm{RPAR}_{\mathrm{clear}}$, at the same location,

$$\mathrm{RPAR}_{\mathrm{cloudy}} = s(F_{\mathrm{cloudy}} - F_{\mathrm{clear}}) + \mathrm{RPAR}_{\mathrm{clear}}, \quad (47)$$

where F_{cloudy} and F_{clear} denote the ratios of direct to total incoming visible radiation under cloudy and clear conditions, respectively. F_{clear} can be determined according to the SZA and aerosol optical depth (cf. Fig. 3). For overcast skies, it is acceptable to assume $F_{\mathrm{cloudy}} = 0$ for most clouds except for very thin clouds of

Figure 10. Same as Figure 8 but for the fixed aerosol optical thickness of 0.225 (solid points) and 1.0 (open points).

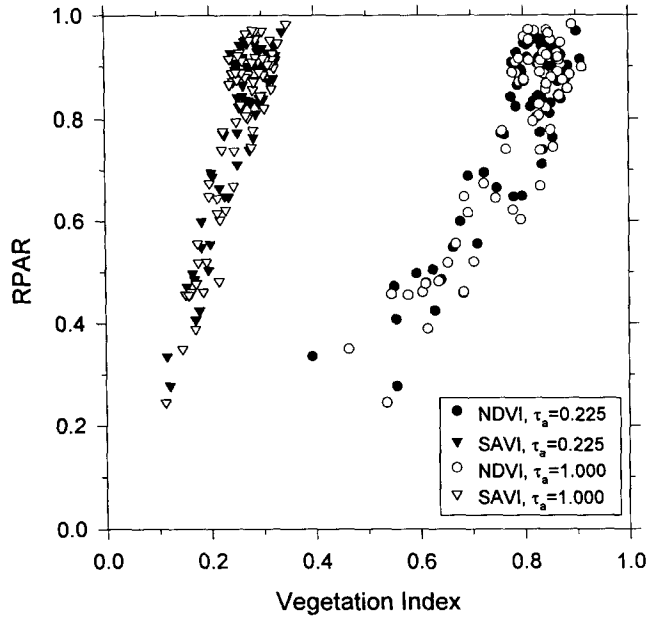

Figure 11. Same as Figure 8 except that all the input parameters are fixed ($r_{g1} = 0.1$, $r_{g2} = 0.12$, $\Lambda = 1.0$, $\theta_s = 30°$) but the optical properties of the leaves which are allowed to change within the ranges given in Table 2.

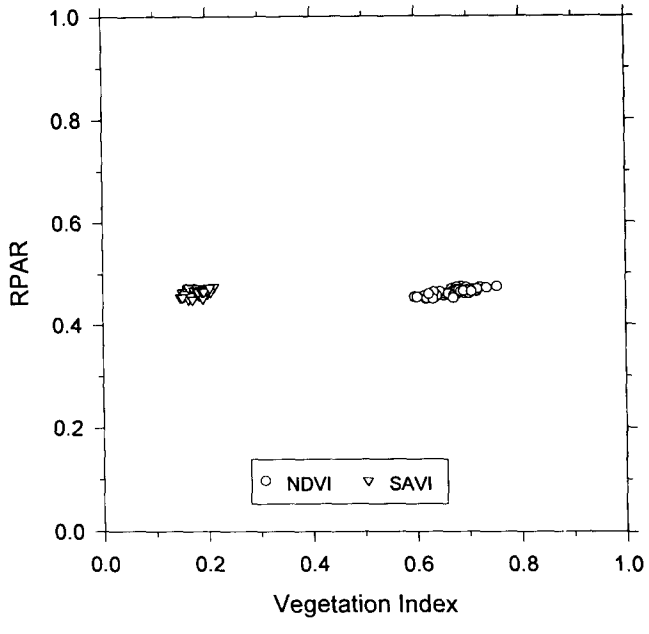

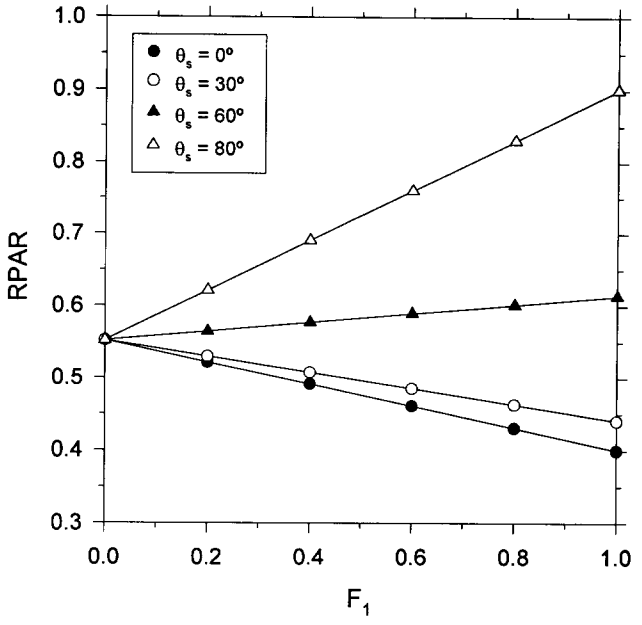

Figure 12. Variation of RPAR with the fraction of direct incoming radiation in the visible band for different solar zenith angles denoted by θ_s.

optical depth well below 10. Determination of F_{cloudy} is more challenging under partially cloudy conditions. The surface insolation retrieving technique of Pinker and Lazslo (1992) can provide the ratio, though the algorithm is quite complex and entails a substantial amount of computations. The efficiency of the adjustment based on Eqs. (46) and (47) is seen by comparing Figure 14 with 15. The values of RPAR shown in Figure 14 are obtained from canopy radiative transfer simulations for

Figure 13. The slope of RPAR vs. F_1 as a function of $RPAR_{clear}$ and cosine of the solar zenith angle.

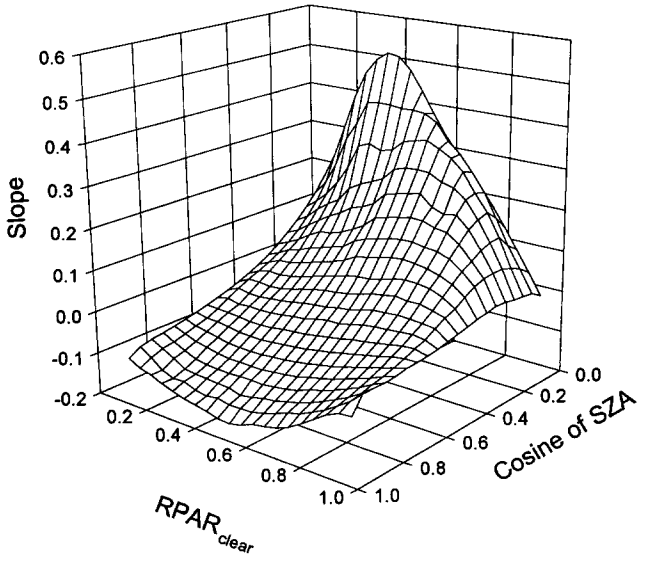

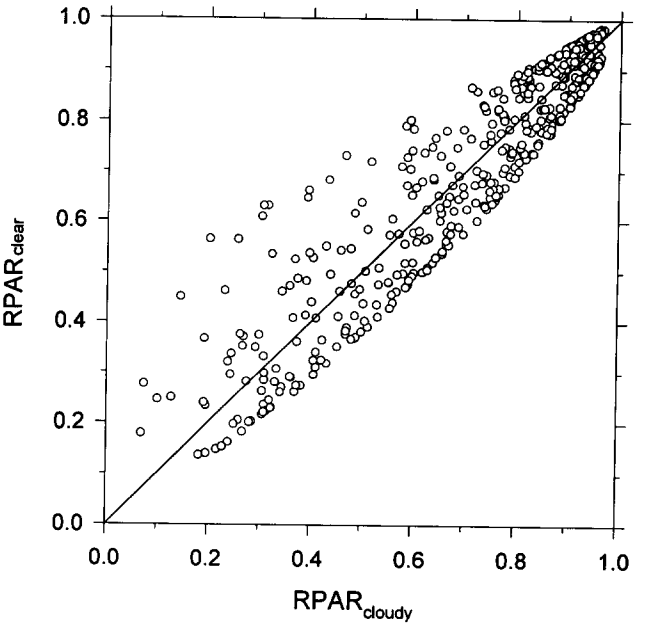

Figure 14. Comparison of the clear-sky and overcast RPAR obtained from canopy modeling. The same random input data are used for the computation of $RPAR_{clear}$ and $RPAR_{cloudy}$ except F_1. The clear-sky F_1 is determined by the solar zenith angle and aerosol whose optical depth is fixed at 0.225, while the overcast F_1 is set to zero.

both clear and overcast skies. All input data are random except for aerosol whose optical depth is set to 0.225. Therefore, F_{clear} is determined by the SZA only, and F_{cloudy} is set to 0. The discrepancies between $RPAR_{clear}$ and $RPAR_{cloudy}$ shown in Figure 14 are exclusively due to the differences between F_{clear} and F_{cloudy}. The differences

Figure 15. Comparison of the overcast RPAR obtained from canopy modeling and estimated from $RPAR_{clear}$ using Eqs. (46) and (47).

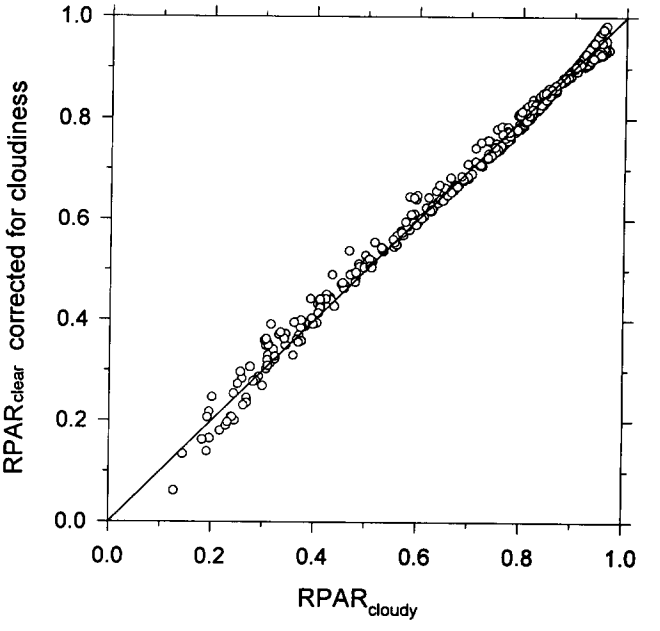

between $RPAR_{clear}$ and $RPAR_{cloudy}$ range approximately from -0.1 to 0.3. Figure 15 compares the overcast RPAR obtained from the simulations and from the clear-sky values of RPAR adjusted to overcast values using Eqs. (46) and (47). The majority of them agree to within 0.05.

ADJUSTING RPAR FOR TIME DEPENDENCY

Although the relationships between RPAR and VIs are not altered by the SZA, RPAR does change with the SZA (except for overcast conditions), as is seen from Figure 16. There are two contradictory factors behind the effect of the SZA on RPAR, namely, the effective LAI and F_1. As the sun approaches the horizon, the interception cross section of the canopy augments, raising RPAR. On the other hand, F_1 diminishes, which helps to lower RPAR (see Fig. 12, SZA = 80°). Since F_1 changes slightly with the SZA for a large range of the SZA (cf. Fig. 2), RPAR keeps increasing with the SZA until the sun becomes very low (SZA $\geq$ 75°) when the F_1 effect dominates. It is also seen from Figure 16 that the change of RPAR with the SZA is more dramatic for low LAI. When the LAI is larger than 5, the variation is almost negligible. This can be explained by the fact that the larger the LAI, the more saturated the canopy absorption tends to be, and thus RPAR is less sensitive to the changes in the interception cross section of the vegetation layer. For SZAs smaller than about 75°, the magnitude and shape of the curves are comparable to the similar plots for FPAR obtained by Goward and Huemmrich (1992). The disparities for larger SZAs are probably because the SAIL model they used does not take into consideration the change of F_1 with the SZA.

Consequently, adjustment for the dependence of RPAR on time is needed, unless RPAR is monitored

Table 3. Numerical Values of the Coefficients of Eq. (48)[a]

		Cosine of Solar Zenith Angle									
RPAR		*0.1*	*0.2*	*0.3*	*0.4*	*0.5*	*0.6*	*0.7*	*0.8*	*0.9*	*1.0*
0.1	*a*	0.266	0.266	0.266	0.266	0.266	0.266	0.266	0.266	0.266	0.266
	b	0.228	0.228	0.228	0.228	0.228	0.228	0.228	0.228	0.228	0.228
	c	0.787	0.787	0.787	0.787	0.787	0.787	0.787	0.787	0.787	0.787
	d	−3.633	−3.633	−3.633	−3.633	−3.633	−3.633	−3.633	−3.633	−3.633	−3.633
0.2	*a*	0.293	0.266	0.266	0.293	0.293	0.293	0.293	0.293	0.293	0.293
	b	0.187	0.228	0.228	0.187	0.187	0.187	0.187	0.187	0.187	0.187
	c	0.818	0.787	0.787	0.818	0.818	0.818	0.818	0.818	0.818	0.818
	d	−1.082	−3.633	−3.633	−1.082	−1.082	−1.082	−1.082	−1.082	−1.082	−1.082
0.3	*a*	0.293	0.293	0.293	0.293	0.293	0.186	0.186	0.186	0.186	0.122
	b	0.187	0.187	0.187	0.187	0.187	0.141	0.141	0.141	0.141	0.124
	c	0.818	0.818	0.818	0.818	0.818	0.912	0.912	0.912	0.912	1.059
	d	−1.082	−1.082	−1.082	−1.082	−1.082	0.358	0.358	0.358	0.358	0.762
0.4	*a*	0.186	0.186	0.186	0.186	0.186	0.122	0.122	0.122	0.122	0.121
	b	0.141	0.141	0.141	0.141	0.141	0.124	0.124	0.124	0.124	0.106
	c	0.912	0.912	0.912	0.912	0.912	1.059	1.059	1.059	1.059	1.007
	d	0.358	0.358	0.358	0.358	0.358	0.762	0.762	0.762	0.762	0.819
0.5	*a*	0.122	0.186	0.186	0.122	0.122	0.121	0.121	0.121	0.121	0.098
	b	0.124	0.141	0.141	0.124	0.124	0.106	0.106	0.106	0.106	0.067
	c	1.059	0.912	0.912	1.059	1.059	1.007	1.007	1.007	1.007	0.886
	d	0.762	0.358	0.358	0.762	0.762	0.819	0.819	0.819	0.819	0.890
0.6	*a*	0.121	0.122	0.122	0.121	0.121	0.121	0.098	0.098	0.098	0.056
	b	0.106	0.124	0.124	0.106	0.106	0.106	0.067	0.067	0.067	0.033
	c	1.007	1.059	1.059	1.007	1.007	1.007	0.886	0.886	0.886	0.795
	d	0.819	0.762	0.762	0.819	0.819	0.819	0.890	0.890	0.890	0.947
0.7	*a*	0.098	0.121	0.121	0.121	0.098	0.098	0.056	0.056	0.056	0.011
	b	0.067	0.106	0.106	0.106	0.067	0.067	0.033	0.033	0.033	0.006
	c	0.886	1.007	1.007	1.007	0.886	0.886	0.795	0.795	0.795	0.741
	d	0.890	0.819	0.819	0.819	0.890	0.890	0.947	0.947	0.947	0.991
0.8	*a*	0.056	0.098	0.098	0.098	0.056	0.056	0.011	0.011	0.002	0.002
	b	0.033	0.067	0.067	0.067	0.033	0.033	0.006	0.006	3E−4	3E−4
	c	0.795	0.886	0.886	0.886	0.795	0.795	0.741	0.741	0.306	0.306
	d	0.947	0.890	0.890	0.890	0.947	0.947	0.991	0.991	0.997	0.997
0.9	*a*	0.004	0.011	0.011	0.011	0.002	0.004	0.004	0.006	0.006	0.009
	b	0.000	0.006	0.006	0.006	3E−4	3E−4	3E−4	3E−4	3E−4	3E−4
	c	0.209	0.741	0.741	0.741	0.306	0.209	0.209	0.152	0.152	0.113
	d	0.995	0.991	0.991	0.991	0.997	0.995	0.995	0.993	0.993	0.991

[a] The typical values of the input parameters used for determining these coefficients are: $r_{g1} = 0.05$, $r_{g2} = 0.055$, $r_1 = 0.084$, $r_2 = 0.442$, $t_1 = 0.059$, $t_2 = 0.514$.

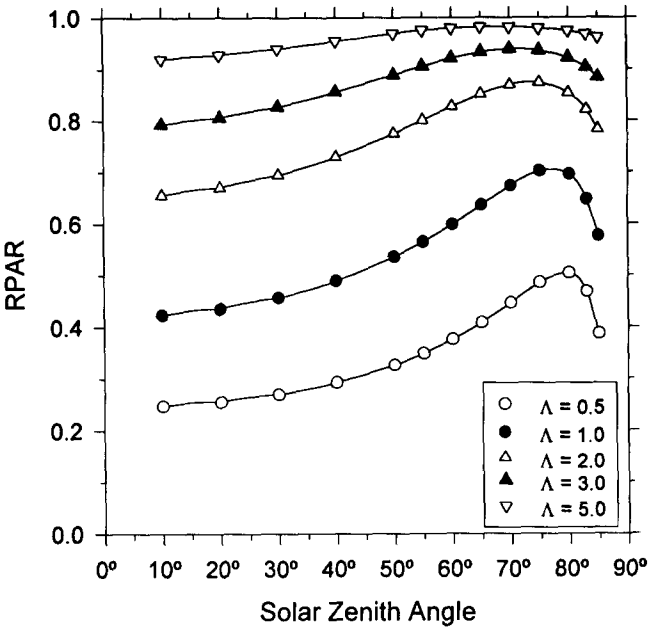

Figure 16. Variation of the clear-sky RPAR with the solar zenith angle for different values of leaf area index denoted by Λ with $r_{gl} = 0.05$, $r_l = t_l = 0.05$.

continuously. Unfortunately, continual observation of RPAR is impossible even if appropriate radiometers were placed on a geostationary satellite with the capability of around-clock monitoring. This is because VIs can only be inferred from satellite data for clear skies, which do not occur constantly. To carry out the correction, the curves in Figure 16 are fitted by the following function:

$$\mathrm{RPAR} = \frac{a}{\mu^c(e^{b/\mu} - d)}, \tag{48}$$

where the values of a, b, c and d are listed in Table 3. From a single instantaneous measurement of RPAR with a known SZA, a set of the coefficients is determined and so is the time (or SZA) dependent function. Using this function, RPAR can be derived at any time. If more than four measurements are available, a more accurate set of parameters can be obtained by fitting Eq. (48) to the data. As mentioned earlier, under overcast conditions, RPAR can be considered independent of the SZA.

SUMMARY AND CONCLUSIONS

We have proposed a new approach to monitor from space the instantaneous amount of photosynthetically active radiation absorbed by canopy ($\mathrm{APAR_{CAN}}$). The major difference between this method and previous ones lies in that $\mathrm{APAR_{CAN}}$ is estimated directly from the reflectance at the top of the atmosphere (TOA) without having to know the incoming PAR at the surface. The method comprises two algorithms. One infers the total PAR absorbed below the top of the canopy (TOC), $\mathrm{APAR_{SFC}}$, and the other distinguishes the fraction of the PAR absorbed by vegetation only. Li and Moreau (1995) have shown how $\mathrm{APAR_{SFC}}$ can be obtained from the reflectance measured at the TOA by virtue of atmospheric radiative transfer simulations. Based on extensive simulation results, a simple parameterization was proposed, which is applicable to both clear and cloudy measurements with three input parameters, namely, the SZA, ozone amount, and aerosol optical properties.

In the present article, a multistream, multilayer canopy radiative transfer model is developed to determine the ratio of the PAR absorbed by the vegetation only over the PAR absorbed below the TOC, RPAR. RPAR is found to correlate well with FPAR, the fraction of the canopy absorbed PAR out of the PAR incident on the surface. One may therefore compute RPAR from FPAR which has been investigated extensively. As an alternative means, estimation of RPAR from the surface vegetation indices (VIs) is examined in more detail. The relationships between RPAR and various forms of VI are obtained from a large number of simulations with the canopy radiation model using random input parameters that cover a wide range of situations. The relationship between RPAR and SAVI turns out to be linear, while the relationship between RPAR and NDVI is better represented by a quadratic equation. Both relationships are nearly insensitive to the solar zenith angle (SZA) and aerosol optical thickness. The influence of soil reflectance on the relationship between RPAR and NDVI is evident but not on the relationship between RPAR and SAVI. The change in leaf area index (LAI) is the driving factor of the corresponding relationships, whereas the diversity of the optical properties of canopy leaves is the major cause of the scatter. The standard deviation of the estimation errors in RPAR from VIs is less than 0.1 using a single regression equation. Although the relationships between RPAR and VIs are not altered by cloud amount and the SZA, RPAR itself is modified by these two factors. Since VI can only be measured by satellite under clear sky conditions, the inferred clear-sky RPAR needs adjustment for use under cloudy conditions. Likewise, corrections are required when the RPAR obtained at a specific time is to be used at other times. Correction models were proposed. The major source of uncertainty in the estimate of RPAR is the same as for the traditional methods, that is, the limited information about the optical characteristics of a canopy, obtained from the TOA reflectance measurements in only two spectral bands, one in the visible and one in the NIR.

In summary, the advantage of this new approach over the traditional one lies in that the PAR absorbed at the surface can be retrieved more readily and accurately than the downwelling PAR, while the accuracies in the estimates of two different ratios (FPAR and RPAR)

required to compute canopy absorbed PAR are comparable. In practice, $APAR_{SFC}$ can be estimated from the TOA visible reflectance regardless of atmospheric and surface conditions. Monitoring RPAR requires clear-sky measurements from both visible and near-infrared sensors, with some ancillary data for atmospheric correction. The clear-sky constraint does not pose a serious problem for RPAR monitoring, since the greenness of a canopy changes gradually and slowly during the growing season. The observation of RPAR can be interrupted by clouds so long as clear-sky measurements are frequent enough to register the evolution of the canopy.

We are grateful to Dr. J. Chen for his review of the draft, Dr. M. Verstraete for his useful comments of the canopy model, and to Dr. J. Cihlar for his encouragement and support.

REFERENCES

Asrar, G., and Myneni, R. (1993), Atmospheric effects in the remote sensing surface albedo and radiation absorption by vegetation canopies, *Remote Sens. Rev.* 7:197–222.

Black, T., Chen, J., Lee, X., and Sagar, R. (1991), Characteristics of shortwave and longwave irradiance under a Douglas-fir forest stand, *Can. J. For. Res.* 21:1020–1028.

Brakke, T., Wergin, W., Erbe, E., and Harnden, J. (1993), Seasonal variation in the structure and red reflectance of leaves from yellow poplar, red oak and red maple, *Remote Sens. Environ.* 43:115–130.

Budyko, M. (1980), *Global Ecology*, Progress Publishers, Moscow.

Cess, R., and Vulis, I. (1989), Inferring surface solar absorption from broadband satellite measurements, *J. Clim.* 2:974–985.

Chen, T., and Ohring, G. (1984), On the relationship between clear-sky planetary albedo and surface albedo, *J. Atmos. Sci.* 41:156–158.

Choudbury, B. (1987), Relationships between vegetation indices, radiation absorption, and net photosynthesis evaluated by a sensitivity analysis, *Remote Sens. Environ.* 2:209–233.

Clevers, J., Van Leeuwen, J., and Verhoef, W. (1994), Estimating the fraction of APAR by means of vegetation indices: a sensitivity analysis with a combined PROSPECT-SAIL model, *Remote Sens. Rev.* 9:203–220.

Dye, D., and Goward, S. (1993), Photosynthetically active radiation absorbed by global land vegetation in August 1984, *Int. J. Remote Sens.* 14:3361–3364.

Goward, S., and Huemmrich, K. (1992), Vegetation canopy PAR absorptance and the normalized difference vegetation index: an assessment using the SAIL model, *Remote Sens. Environ.* 39:119–140.

Goward, S., Huemmrich, K., and Waring, R. (1994), Visible–near infrared spectral reflectance of landscape component in western Oregon. *Ecol. Appl.* 4:322–343.

Hall, F., Huemmrich, K., Goetz, S., Sellers, J., and Nickeson, J. (1992), Satellite remote sensing of surface energy balance: success, failures and unresolved issues in FIFE, *J. Geophys. Res.* 97D:19,061–19,089.

Huete, A. (1988), A soil adjusted vegetation index (SAVI), *Remote Sens. Environ.* 25:53–70.

Koepke, P. (1989), Removal of atmospheric effect form AVHRR albedos, *J. Appl. Meteorol.* 28:1341–1348.

Li, Z., and Garand, L. (1994), Estimation of surface albedo from space: a parametrization for global application, *J. Geophys. Res.* 99D:8335–8350.

Li, Z., and Moreau, L. (1995), A new approach for remote sensing of canopy absorbed photosynthetically active radiation. I: Total surface absorption, *Remote Sens. Environ.*, 55: 175–191.

Masuda, K., Leighton, H., and Li, Z. (1995), A new parameterization for the determination of solar flux absorbed at the surface from satellite measurements, *J. Clim.*, 8:1615–1629.

Myneni, R., and Williams, D. (1994), On the relationship between FAPAR and NDVI, *Remote Sens. Environ.* 49:200–211.

Myneni, R., Asrar, G., and Tanré, D., and Choudbury, B. (1992), Remote sensing of solar radiation absorbed and reflected by vegetated land surfaces, *IEEE Trans. Geosci. Remote Sens.* 30:302–314.

Nilson, T. (1971), A theoretical analysis of the frequency of gaps in plant stands, *Agric. Meteorol.* 8:25–38.

Norman, J. (1979), in *Modification of the Aerial Environment of Plants* (B. Barfield and J. Gerber, Eds.), American Society of Agricultural Engineers, Section 3.6.

Pinter, P. (1993), Solar angle independence in the relationship between absorbed PAR and remotely sensed data for alfalfa, *Remote Sens. Environ.* 46:19–25.

Pinker, R., and Lazlo, I. (1992), Modelling surface solar irradiance for satellites applications on a global scale, *J. Appl. Meteorol.* 31:194–211.

Prince, S. (1991), A model of regional primary production for use with coarse resolution satellite data, *Int. J. Remote Sens.* 12:1313–1330.

Sellers, P. (1985), Canopy reflectance, photosynthesis and transpiration, *Int. J. Remote Sens.* 6:1335–1372.

Verstraete, M. (1987), Radiation transfer in plant canopies: transmission of direct solar radiation and the role of leaf orientation, *J. Geophys. Res.* 92D:10,985–10,995.

Verstraete, M. (1988), Radiation transfer in plant canopies: scattering of solar radiation and canopy reflectance, *J. Geophys. Res.* 93D:9483–9494.

Walter-Shea, E., and Norman, J. (1991), in *Photon–Vegetation Interactions* (R. Myneni and J. Ross, Eds.), Springer-Verlag, Berlin, Heidelberg, New York, Chap. 8.

Walter-Shea, E., Blad, B., Hays, C., Mesarch, M., Deering, D., and Middleton, E. (1992), Biophysical properties affecting vegetative reflectance and absorbed photosynthetically active radiation at FIFE site, *J. Geophys. Res.* 97D:18,925–18,934.

WCP (1986), A preliminary cloudless standard atmosphere for radiation computation, Association for Meteorology and Atmospheric Physics Radiation Commission, WCP-112, Geneva, Switzerland.